Catal Lett (2007) 119:50–58
DOI 10.1007/s10562-007-9184-8

Fabrication of an Effusive Molecular Beam Instrument for Surface Reaction Kinetics—CO Oxidation and NO Reduction on Pd(111) Surfaces

Kandasamy Thirunavukkarasu · Chinnakonda S. Gopinath

Received: 13 May 2007 / Accepted: 22 June 2007 / Published online: 14 July 2007

Abstract A simple molecular beam instrument (MBI) was fabricated for measuring the fundamental parameters in catalysis such as, sticking coefficient, transient and steady state kinetics and reaction mechanism of gas/vapor phase reactions on metal surfaces. Important aspects of MBI fabrication are given in detail. Nitric oxide (NO) decomposition and NO reduction with carbon monoxide (CO) on Pd(111) surfaces were studied. Interesting results were observed for the above reactions and they support the efficiency of the MBI to derive the fundamental parameters of adsorption and catalysis. Sustenance of CO oxidation at 400 K is dependent mostly on the absence of CO-poisoning; apparently, CO + O recombination is the rate determining step ≤400 K. NO adsorption measurements on Pd(111) surface clearly indicating a typical precursor kinetics. Displacement of the chemisorbed CO by NO on Pd(111) surfaces was observed directly with NO + CO beams in the transient kinetics. It is also relatively easy to identify the rate-determining step directly from the MBI data and the same was demonstrated for the above reactions.

Keywords Molecular beam · Kinetics · Catalysis · Nitric oxide · Carbon monoxide · Pd(111)

1 Introduction

The concepts and principles of heterogeneous catalysis are yet to be understood thoroughly at molecular level. As the industrial catalysts have complex heterogeneous structures on their surfaces, simple model catalysts should be used to understand a catalytic reaction at molecular level. Moreover, there are number of practical difficulties to use real-world catalysts in surface science studies. Surface science studies generally carried out under ultrahigh vacuum (UHV) conditions to maintain collision-free conditions for employing in-situ electron/ion/photon based techniques. The pressure and material gaps arise when a complex industrial catalytic process occurs at atmospheric or high pressure and model catalytic studies that are carried out under UHV conditions. In practice, a model single crystal catalyst, having a homogeneous surface and a very low surface area in a particular planar orientation, is used to get the molecular details of heterogeneous catalytic reactions [1–6]. Complexities can be introduced to a model single crystal catalyst, like introducing a promoter, like potassium, and, an inhibitor, like sulfur [7–10] and the influence of them on the catalyst can be studied. Metal atoms deposited on an oxide support have been used as a model catalyst for the last two decades, [11–15] which also have a low surface area. Somorjai and his group [16, 17] synthesized a three-dimensional model catalyst with high-surface area (400 m^2/g) for surface science studies. However, much more needs to be carried out to solve the pressure and material gap problem, which is being pursued by few research groups [7–17]. In any case, model studies using metal single crystals are necessary, particularly in cases, when a complex catalytic reaction is employed [18].

Molecular beam, which is a directed and spatially defined flux of molecules [19], could be employed to create high surface coverage. The advantages of molecular beams for kinetic measurements were recently reviewed by three different groups [14, 20–22]. Important advantages of molecular beams are summarized below: (a) high surface coverage

K. Thirunavukkarasu · Chinnakonda S. Gopinath (✉)
Catalysis Division, National Chemical Laboratory,
Dr. Homi Bhabha Road, Pune 411 008, India
e-mail: cs.gopinath@ncl.res.in

can be achieved on the metal substrates without flooding the UHV chambers; (b) Molecular beams minimize the re-adsorption of reactant gases compared to the conventional experiments, due to single scattering conditions, and (c) a pressure difference of up to seven orders of magnitude [23] between the pressure on the sample surface and the background can be maintained in these experiments. Recently, a simple thermal molecular beam instrument (MBI) was fabricated [24] in our laboratory for surface reaction kinetic studies, and particulars of the fabrication are described in detail. CO oxidation, NO adsorption, and NO + CO reaction on Pd(111), which are important reactions from environmental point of view and technically relevant to the automotive catalytic converters, were studied successfully using MBI and important results are discussed here [24].

NO reduction and CO oxidation reactions are important processes in pollution control especially in automobiles. In the last decade palladium only three-way catalytic (TWC) converters (Pd supported on γ -alumina support) on a wash coat were introduced, replacing the traditional Rh–Pt catalysts, because of its reasonable performance to reduce NO in net oxidizing conditions, its low cost and better abundance than Rh. Hence an understanding of NO_x reduction reactions under net oxidizing conditions on palladium catalysts is attracting more attention for the last one decade [25]. Although number of reports are available in the literature on NO reduction catalytic activity on Pd on different supports [11, 13, 26, 27], there is a serious lack in understanding the reaction kinetics at atomic/molecular level. Our studies on these reactions on Pd(111) through MBI contributed some light on the mechanistic aspects of the reactions and the same are discussed below.

2 Fabrication of Molecular Beam Instrument (MBI) for Kinetic Studies

2.1 Design Considerations MBI Chamber

A 12 L capacity stainless steel UHV chamber houses all necessary accessories to create molecular beam and evacuated with a 210 L/s turbo-molecular drag pump (Pfeiffer, TMU261) to a base pressure of about 3×10^{-10} Torr. MBI is equipped with a molecular beam doser setup, which is described in the next section and a sputter ion gun (AG5000, VG Scientific) placed exactly opposite to each other at 180° apart (Fig. 1). An xyz-manipulator with a rotary platform for mounting the Pd(111) sample on a power-thermocouple feed-through (Caburn, 30 A-DC and 5 KV) is placed perpendicular to the doser and sputter ion set-up so that the sample can be moved in all three direction and rotated 360°. The above feed-through is connected to liquid nitrogen well. Thus the crystal can be cooled to about 110 K with liquid nitrogen and resistively heated to 1,373 K by home-built temperature controller. A stationary quadrupole mass spectrometer (Pfeiffer, Prisma QMS 200M3), which can detect gas phase species up to 300 amu, and a cold cathode ion gauge (Pfeiffer, IKR270) for measuring the chamber pressure are connected opposite to each other and away from the beam doser. The mass spectrometer is kept out of the line-of-sight of the Pd(111) sample to avoid any angular desorption effects. Thus both the QMS and cold cathode ion gauge were kept at the same distance from turbo pump to minimize the difference between the total pressure readings. Due to the above geometrical constraints a lowest reaction probability of 0.001 mL/s can be measured. The Pd(111) single crystal sample was mounted by spot-welding a 0.5 mm thick tantalum wire on the backside of the crystal and connected to a pair of copper rods, which in turn were connected to the above power-thermocouple feedthrough. A K-type thermocouple was welded on the periphery of the crystal and to the thermocouple leads of the feed-through. The present set-up is based on the extension of the King and Well's method [28].

2.2 Design Considerations of the Doser Assembly

Clausing's work [29] introduced the details of molecular flow in a capillary tube. Low energy molecular beams can be created by an array of these microcapillary tubes [30]. Collimated gas beams are the main part of many important experimental techniques in molecular physics, mechanism of chemical reactions, many spectroscopic techniques, surface science and epitaxial growth of crystals [31]. Particularly molecular beams are extensively used in surface science studies [11, 13, 14, 18, 20–24, 32, 33].

Molecular beam doser consists of a multichannel array of capillary disk with open segment of disk diameter to the sample (10 mm) is larger than that of the sample (dia = 8 mm). An important concept in describing the quality of a doser, the enhancement factor (E), which is the ratio between the true flux at the sample due to the molecular beam and the gas flux due to background gas pressure P, is calculated by the following expression [34].

$$E = 1 + fS/[k_B T(1 - fs)v_c A] \quad (1)$$

where, v_c = velocity of the gas molecules, $v_c = (2\pi m k_B T)^{\frac{1}{2}}$, f = fraction of the beam intercepted by the sample, S = pumping speed, k_B = Boltzmann constant, T = temperature of the gas molecules, s = sticking probability of the molecules, A = surface area of the sample, and m = mass of the gas molecules. Aspect ratio calculation of microcapillaries, which is capillary length (L) to diameter (a) ratio, decides the beam profiles. For microcapillary beam doser with an aspect ratio >40, there would be no considerable beam profile changes except a reduction in conductance with increasing

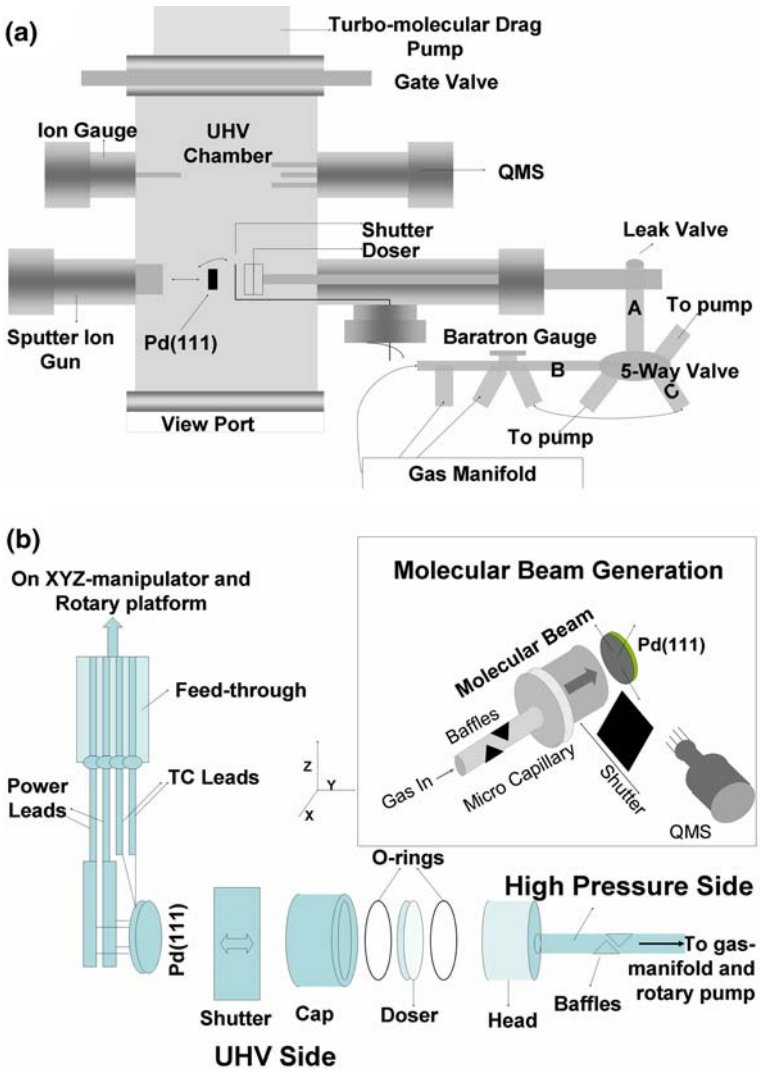

Fig. 1 (**a**) Schematic representation of a top view of molecular beam instrument; (**b**) Schematics of doser assembly of MBI and the inset show the generation of molecular beam

ratio. In the present case we have employed an aspect ratio of 100. Guevremont et al. [35] showed that the flattening of the beam profile was widely spread for a microcapillary with a = 10 μm than that of a larger diameter (a = 50 μm) with same lengths of capillary (L = 2 mm), but a reduction in conductance was observed with a = 10 μm capillary array and good beam quality. Indeed the present design provides uniform flux on the overall surface of the metal substrate of 8 mm diameter [24].

The molecular beam doser consists of a 13 mm disk multichannel array made up of microcapillary glass tubes of 1 mm in length and 10 μm in diameter each (Collimated Holes Inc.). The doser is attached through a threaded cap and head with teflon O-rings. It is to be mentioned that the open portion of the above microcapillary is only 10 mm. A quarter inch tube (OD) of 15 cm in length with baffles (shown in Fig. 1b) to avoid the gas acquiring the shape of the tube is attached with the beam-doser head. Thus a minimum dead volume and a minimum gas load can be maintained in the present set-up compared to a recently reported beam doser [36]. A laterally movable stainless steel shutter is placed between the microcapillary doser and the Pd(111) crystal in order to interrupt the beam at will (Fig. 1b inset). Hence we could maintain a minimum of 5 mm doser to sample distance in our present setup, which gives an enhancement factor (E) of ~12 [24] and ~45% fraction of the beam (f) impinges on the surface.

Cyclohexane condensation was performed at 125 K (Fig. 2) for the calculation of f value, the fraction of the beam intercepted by the sample, which is an important factor for calculating the adsorbate coverage at time, t [37].

$$\theta(t) = \frac{N(t)}{A} = \frac{1}{A}\int_0^t [\alpha \Delta P(\tau) + \beta s(\tau) P(\tau)]\mathrm{d}t \qquad (2)$$

where, $N(t)$ = number of adsorbate molecules, A = surface atom density of the Pd(111) sample (surface atom density

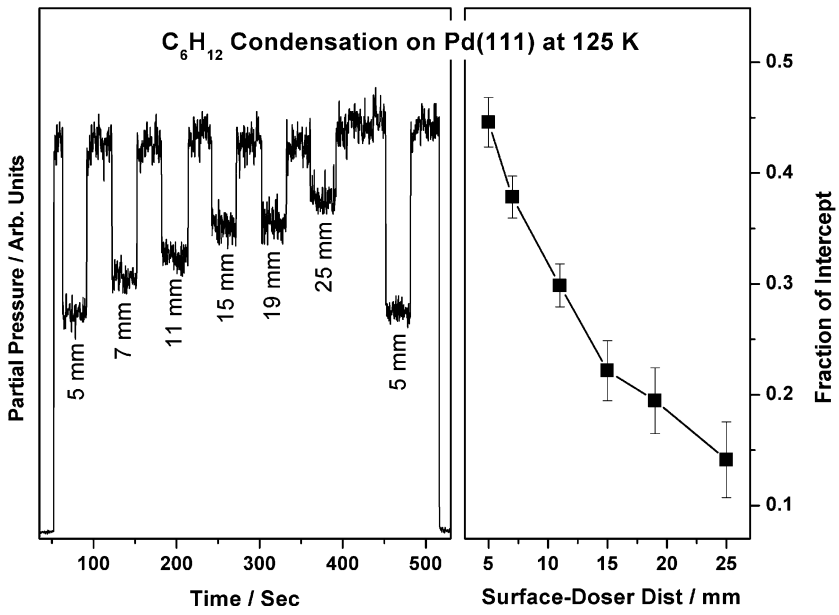

Fig. 2 Cyclohexane uptake/condensation on Pd(111) surface as a function of distance between the doser assembly and the crystal surface at 125 K

of Pd = 1.53×10^{15} cm^{-2}), α, β are constants and independent of the beam flux, sample-to-surface distance and surface temperature. It is to be noted that sticking probability of cyclohexane is assumed to be unity at 125 K. Calculated value for α and β is 2.99×10^6 molecules/g and 1.76×10^5 molecules/g, respectively, for our present MBI set-up [24]. The pumping rate is determined by means of the following equation [39].

$$\rho = \rho_o \exp\left[-\left(\frac{\Lambda RT}{V}\right)t\right] \tag{3}$$

where ρ, ρ_o, Λ and V represent the pumping rate, pumping coefficient, pumping constant and volume of the chamber, respectively.

The gas-flux in the molecular beam is determined and controlled by the precision leak-valve opening and the backing gas pressure in the gas-manifold. The gas-flux is set by setting both the precision leak valve, and the backing gas pressure in volume B (Fig. 1), which is measured by a MKS Baratron pressure gauge initially calibrated against the equilibrium vapor pressure of water at different temperatures. For flux dependent measurements, normally the backing pressure varied and the precision leak valve-opening kept at a predetermined position.

The metal substrate, an 8 mm diameter Pd single crystal cut in the (111) direction was used as supplied (Metal Crystals and Oxides Ltd., Cambridge), was mounted by the method described above. The crystal is cleaned in-situ by a combination of argon ion sputter-anneal cycles at 1,000 K in oxygen atmosphere and oxygen treatments at 1,000 K followed by flashing to 1,200 K before each experiment as described by Ramsier et al. [26]. The cleanliness of the sample was verified by recording standard temperature programmed desorption (TPD) measurements after adsorption of NO or CO and reproducible CO oxidation kinetics.

3 Catalytic Converter Reactions on Pd(111) Surfaces

3.1 CO Oxidation

All the results reported in this manuscript were carried out by following the procedure under isothermal conditions given in Fig. 3 for CO oxidation. For all experiments Pd(111) was kept at desired constant temperature and exposed to CO + O_2or NO or NO + CO beam of desired composition. The partial pressure of all the relevant mass species was recorded as a function of time. Figure 3 shows a typical raw kinetic data obtained by exposing (a) 4:1 CO:O_2 beam and (b) 1:4 CO:O_2 beam on clean Pd(111) surface kept at 400 K. A series of actions were taken during these experiments are described below: (1) the CO:O_2 beams were turned on at t = 10 s, after recording the background intensity of the relevant mass species for a short while. At this point reactant molecules (CO and O_2) are scattered in the UHV chamber. An immediate increase in the partial pressures of CO and O_2 could be clearly seen and their partial pressure values increase up to a new steady-state value. It is to be noted that the partial pressure of CO_2 does increase at this point due to the reaction between the reactants adsorbed from background on the Pd(111) surface. This represents a maximum of 4% of the total rate and not included in the data analysis. (2) Around t = 13 s the shutter, till then blocking the molecular beam

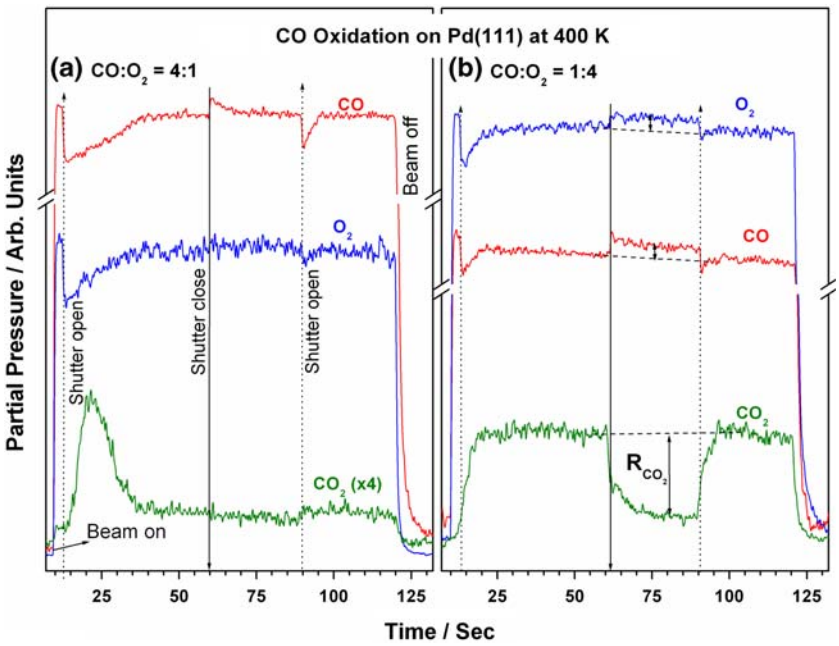

Fig. 3 Experimental data from a typical isothermal kinetic test described in the text carried out with CO + O_2 at 400 K for (**a**) 4:1 CO:O_2 beam composition (CO-rich); (**b**) 1:4 CO:O_2 beam composition (O_2 -rich)

from impinging the Pd(111) surface directly, was removed to allow for direct adsorption of reactants on the surface. An instantaneous decrease in the partial pressure of the reactants was observed and along with a slow increase in the CO_2 partial pressure. This stage is termed as the transient state (TS) and will be discussed in detail later. A careful look at the CO_2 evolution data exhibit about 2 s delay (Fig. 3a) in starting the CO_2 production, although CO and O_2 adsorbs at the point of shutter removal. Similar observations has been made by Burghaus et al. [40] on oxygen pre-covered surfaces of Pd(111) and Pd(110). (3) The CO + O_2/Pd(111) system is allowed to evolve until a steady state (SS) is reached, which normally occurs within 30 s after shutter removal; in the present example in Fig. 3b SS reaches around $t = 20$ s (5 s after shutter opening). However, with CO:O_2 (4:1) beam SS reaches around $t = 40$ s. (4) In the SS the MB was deliberately blocked between $t = 60$ and 90 s to measure the steady state rate of the reaction. There is a clear increase in the partial pressure of CO and $O_2$and a drop in CO_2 partial pressure (Fig. 3b), shown by double headed arrow. A new SS reaches in few seconds after blocking the beam. CO_2 partial pressure shows a sudden drop at the instance of beam blocking followed by a slow decay for the next 5 s. Indeed, the above observation of slow CO_2 decay in the SS varies with reaction temperatures and beam compositions. (5) After about 30 s from the blocking of the beam, the shutter was removed again at $t = 90$ s and again the reaction is allowed to return to the earlier SS mentioned in point 3. (6) The beam was turned off at 120 s. In some special cases, where oxygen atoms left-over the surface, CO titration was performed to measure the surface-oxygen coverage after the reaction [24].

It is to be noted that the sustenance of CO oxidation in the SS with CO:O_2 1:4 beam and not with CO-rich CO:O_2 4:1 beam. Indeed the CO_2 production observed in the TS in Fig. 3a is due to the oxygen adsorption after shutter removal at $t = 13$ s. However, unlike with CO:O_2 (1:4) (Fig. 3b), no net O_2 adsorption could be observed in the SS; especially no pressure change observed for oxygen and carbon dioxide in the SS demonstrate the poisoning of the surface Pd by large CO-coverage. In fact an increase (decrease) in CO partial pressure observed at the time of shutter blocking (opening) in the SS at $t = 60$ (90) s is due to some CO-desorption (adsorption) suggesting a dynamic CO-coverage occurring on the surface till the beam is on. Nonetheless, pressure changes observed in the SS during the beam-blocking period (Fig. 3b) is due to the sustenance of the reaction. Indeed the above pressure changes observed directly provides the SS-rate of the reaction, of course, after mass intensity calibration [24]. SS rate observed in Fig. 3b suggests excess oxygen does not poison the surface, rather facilitate the reaction at the same temperature (400 K). Slow CO_2 pressure decay (step 4) followed by fast change at the point of beam blocking at $t = 60$ s observed in the SS (Fig. 3b) is attributed to the recombination of CO + O species at ≤400 K on Pd(111) surfaces. Indeed the fast changes observed in CO and O_2 partial pressures hint that adsorption of reactants is a fast step. Slow rise in CO_2 partial pressure after the shutter removal in the TS and SS supports the above point.

3.2 NO Adsorption

Figure 4a shows the NO uptake from NO beam on Pd(111) as a function of substrate temperature. Experiments were also carried out without opening the shutter as a reference experiment to find out the extent of NO uptake without any fitting protocols and within the experimental error limits. A simple difference between the reference and actual experiments and the integration provides the coverage and sticking probability of NO (s_{NO}) as a function of time, of course after the calibration of mass spectrometer signals. s_{NO} on Pd(111) was calculated using the formula [37].

$$s(t) = \frac{1}{f}\frac{\Delta P(t)}{P_{eq}(t) - P_{base}(t)} \tag{4}$$

where, f is the fraction of the beam intercepted by the crystal, $\Delta P(t)$ is the difference between the equilibrium partial pressure of NO ($P_{eq}(t)$) and the observed partial pressure of NO and $P_{base}(t)$ is the base pressure of NO. Figure 4b shows the temperature and θ_{NO} dependence of s_{NO} on Pd(111). Briefly, s_{NO} is directly proportional to the change in pressure due to NO uptake on Pd(111) after shutter removal with respect to the total pressure. Once the beam directly impinges on the surface, a large pressure difference on the sample surface and the background and drifting of NO molecules in the background towards turbo pump due to pressure gradient makes the adsorption from background negligible. In other words, a single scattering condition with no re-adsorption from background occurs at this stage. Furthermore, s_{NO} (0.5) is inversely proportional to the fraction of the beam intercepted, which is 25% in the present case. Estimated error margin of s_{NO} values from the uptake measurements is up to 5% and should be considered for any purpose. A time evolution of s_{NO} was calculated first from the experimental NO uptake on Pd(111) data, given in Fig. 4a, and converted in terms of NO-coverage (θ_{NO}). The initial s_{NO} is constant between 300 and 425 K and decreases at temperatures higher than 425 K. A maximum $s_{NO} = 0.5$ was observed at low temperatures between 300 and 350 K on clean Pd(111) up to 70–80% of the saturation coverage. This behavior is typical of precursor-mediated adsorption. At high temperature, the adsorption plateau becomes smaller due to faster desorption and phenomenologicallly a description of s_{NO} on the basis of a Langmuir model becomes more appropriate. Very similar trend in s_{NO} on Pd(110) surface was reported by Sharpe and Bowker [41] and indicates the lifetime of chemisorbed NO species decreases linearly with increasing temperature on Pd(111) and Pd(110).

3.3 NO + CO Reaction

Molecular beam with more than one reactant or component can be prepared with different compositions and hence a possible catalytic reaction on adsorption on metal surfaces could be studied with MBI. NO + CO reaction was carried out on Pd(111) surfaces under isothermal conditions at different temperatures, with mixed NO:CO beam as a function of beam compositions, beam fluxes, and substrate temperature [24]. Two important aspects of NO displacing CO in the transient state, steady state rate of the reaction and hence stoichiometry of the same is reported here.

3.3.1 Transient Kinetics—Displacement of CO_{ads} by NO

Raw transient kinetic data obtained from NO:CO (2:1) reaction on Pd(111) surface at 375 K is shown in Fig. 5a. Dotted line shown is the reference experiment carried out without removing the shutter in the transient state, mainly to employ as background for those experiments reported for all the calculation purposes. NO adsorption trend follows the expected behavior at all of the temperatures and compositions. An initial drop in the partial pressure is

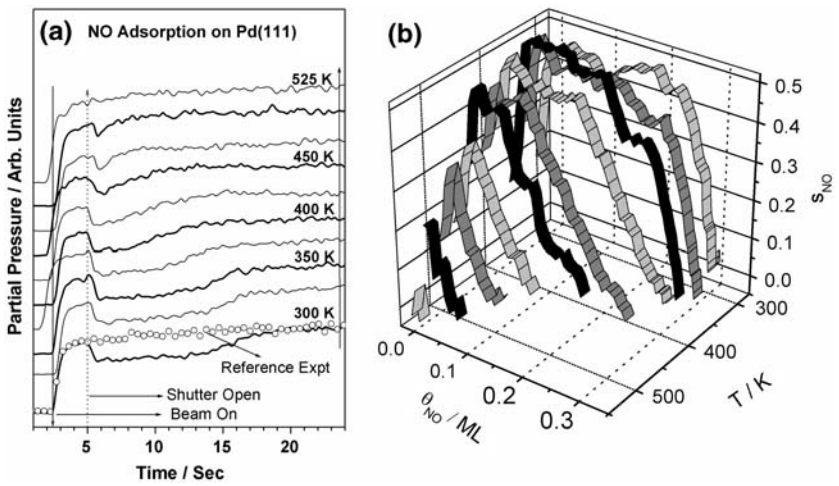

Fig. 4 (**a**) NO uptake on Pd(111) from ^{14}NO molecular beam as a function of time and temperature; (**b**) Temperature dependence of accumulated NO coverage (θ_{NO}) and sticking coefficient calculated from the NO uptake data. Note the same initial sticking coefficient is maintained between 300 and 425 K up to about 80% saturation coverage for adsorption temperatures at 300 and 325 K

observed upon shutter removal due to initial NO uptake on Pd(111) and a subsequent asymptotic approach to the steady state. The time evolution of the partial pressure of CO is more complex (Fig. 5a). An immediate drop in the partial pressure upon unblocking the beam was observed, followed by an increase in the partial pressure after few seconds demonstrating a clear desorption. It indicates that a large amount of CO is displaced by NO due to its preferential adsorption and strong chemisorption on Pd(111) compared to CO. The CO_{ads}, CO_{des}, and NO_{ads} coverages were obtained by integrating the area of the adsorption and desorption in the transient state as shown in Fig. 5a with different shades and the above coverages are given in terms of monolayers in Fig. 5b. This effect was observed clearly for all of the beam compositions at 375 K. NO_{ads} decreases linearly as the beam becomes CO-rich. Initial CO_{ads} also increases with the CO-rich beams. However the amount of CO_{des} indicates that the CO displacement is very strong for NO-rich beams and the same gradually decreases as the beam becomes richer in CO. For CO-rich beam compositions the process is slower since the CO displacement is directly proportional to F_{NO}. Generally, as the beam becomes richer in CO, (or poor in NO), the displacement of CO molecules takes a longer time. Only minor CO-displacement was observed for 1:15 NO:CO beam. CO displacement effect by NO on Pd(111) was observed up to 475 K [32]. At temperatures ≥525 K the displacement effect was very poor or not observed due to the very small steady state coverage of the reactants, particularly CO.

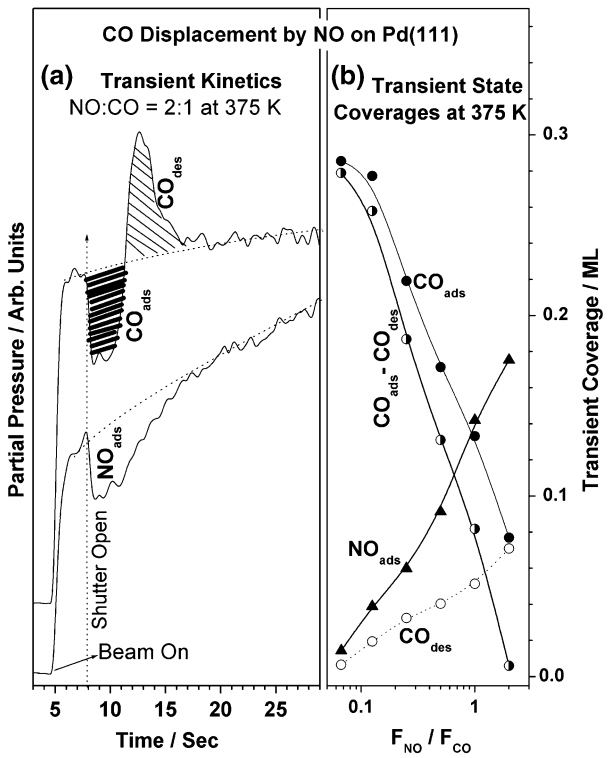

Fig. 5 (**a**) Coverage of NO and CO in the transient state by dosing NO + CO (2:1) beam on Pd(111) at 375 K. Reference experiments carried out without removing the shutter is denoted by dotted line. NO_{ads}, CO_{ads}, and CO_{des} correspond to the coverage of NO and CO and coverage of desorbed CO in the transient state, respectively; (**b**) Coverages of NO and CO, CO_{des} and effective CO coverage is shown for different NO:CO ratios at 375 K

The displacement of a chemisorbed species by another incoming species has been suggested and observed by few groups [42–46] for various catalytic reactions. It is also clear from the above observations that the adsorption of NO on Pd(111) is dominating and hence an enrichment of NO over CO occurs compared to the gas phase [32]. A similar effect has already been observed by Gopinath and Zaera on Rh(111) [46]. The present results reveal a clear difference between adsorbate composition on the surface and beam compositions with respect to both the reactants. It is important to note that the actual surface coverage decides the course of the reaction. Such direct information is crucial to understand the catalysis phenomenon, since most of the reactions employ more than one reactant.

3.3.2 Temperature Dependence on Rate of NO + CO/Pd(111)

The temperature dependence of molecular beam kinetics in the steady state for the production of N_2, N_2O, and CO_2 for 1:4 NO:CO beam composition was studied, as a continuation of transient kinetics discussed above. Figure 6 shows the rate of formation $2N_2 + N_2O$, N_2O, and CO_2 measured in the steady-state for 1:4NO:CO composition at a total flux (F_{NO+CO}) of 0.25 mL/s. It reveals that no effective NO + CO reaction on Pd(111) was observed within the detection limits of QMS below 425 and above 625 K. The active temperature window for NO reduction lies between 425 and 575 K with a maximum steady-state rate around 475 K. The N_2O production rate is about an order of magnitude lower than that of N_2 production. At temperatures > 525 K, the overall rate slowly decreases and no N_2O production can be observed.

Figure 6 shows the rate of formation $2N_2 + N_2O$, N_2O, and CO_2 measured in the steady-state for 1:4 NO:CO composition at a total flux (F_{NO+CO}) of 0.25 mL/s. Needless to say that the nitrogen molecule formation requires the dissociation of two NO molecules and hence the rate is multiplied by a factor of 2. At a reaction temperature of 475 K, a maximum productivity is observed for the major products N_2 and CO_2. There is a clear decrease in the reaction rate on either side of 475 K. In fact the above steady-state rate data is plotted in Fig. 6 in such a manner that rate of all of the reduced products are added ($2R(N_2) + R(N_2O)$) and compared to that of oxidized product, R_{CO_2}, to substantiate the redox nature of the

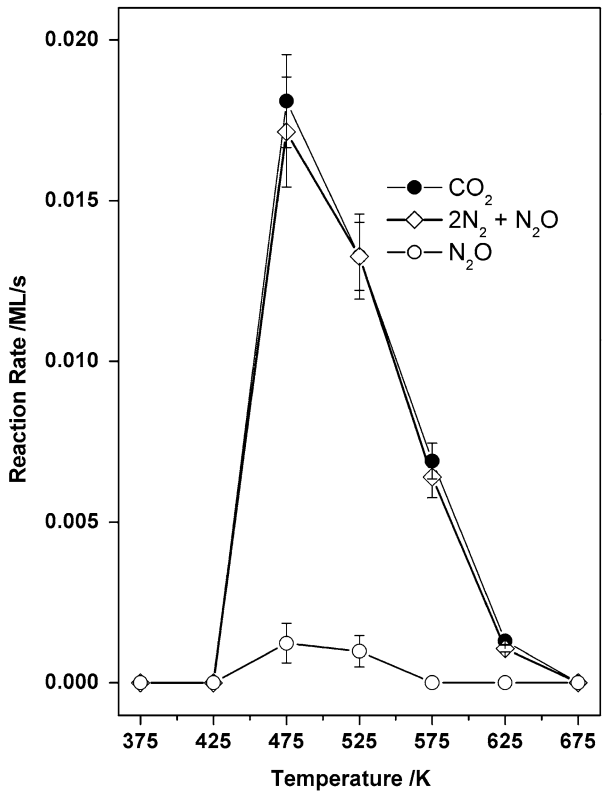

Fig. 6 Steady state rate of NO + CO reaction for NO:CO (1:4) beam composition is plotted as a function of temperature for CO_2 and nitrogen containing products. This figure clearly reveals that the stoichiometry of the product formation. i.e., $R(CO_2) = 2R(N_2) + R(N_2O)$

reaction as well as to confirm the consistency in the experimental data through Eq. 5.

$$R(CO_2) = 2R(N_2) + R(N_2O) \quad (5)$$

A good overall correspondence is observed between the rate of CO oxidation and nitrogen containing products formation suggesting that the data is self-consistent within the experimental error limit. Indeed the above agreement holds good for other NO:CO beam compositions also [24, 32].

4 Conclusions

Basic design considerations for a thermal MBI unit were discussed elaborately. The implications of doser design were presented. In general, gas phase reaction on metal surface can be studied with MBI. CO oxidation, NO decomposition, and NO + CO reaction on Pd(111) were carried out and interesting new insights of the reaction were brought out due to the employment of MBI. Sustenance of CO oxidation on Pd(111) surfaces at 400 K is shown to be dependent on the CO-poisoning. Further, CO + O recombination seems to be the rate determining step for the overall CO-oxidation under the conditions studied. NO adsorption kinetics on Pd(111) indicate that NO dissociation starts on Pd(111) surfaces > 400 K. Sticking coefficient measurements show $s_{NO} = 0.5$ and the NO adsorption trend indicating the precursor mediated adsorption. Direct displacement of CO_{ads} by NO was observed between 375 and 475 K and the transient state coverage calculations show that the surface composition was significantly different from the NO:CO beam composition.

Acknowledgments We thank Profs. H-J. Freund and J. Libuda for co-operation and helpful discussions. CSG gratefully acknowledges Volkswagen foundation and Alexander von Humboldt foundation for financial support to build the molecular beam instrument at National Chemical Laboratory, Pune, India. CSG also thanks Royal Society-British Council for funding a bilateral project. KT thanks CSIR, New Delhi, for a research fellowship.

References

1. Langmuir I (1922) Trans Faraday Soc 17:607
2. Ribeiro FH, Gerken CA, Rűpprechter G, Somorjai GA, Kellner CS, Coulston GW, Manzer LE, Abrams L (1998) J Catal 176:352
3. Bonzel HP, Krebs HJ (1982) Surf Sci 117:639
4. Bonzel HP (1987) Surf Sci Rep 8:43
5. Nørskov JK, Holloway S, Lang ND (1984) Surf Sci 137:65
6. Groff A (1998) Appl Phys A 67:627; Gravil PA, Toulhoat H (1999) Surf Sci 430:176
7. Campbell CT, Goodman DW (1982) Surf Sci 123:413
8. Goodman DW, Kiskinova M (1981) Surf Sci 105:L265
9. Kiskinova M, Goodman DW (1981) Surf Sci 108:64
10. Goodman DW (1984) Appl Surf Sci 19:1
11. Freund H-J, Bäumer M, Libuda J, Risse T, Rupprechter G, Shaikhutdinov S (2003) J Catal 216:223; Hoffmann J, Meusel I, Hartmann J, Libuda J, Freund H-J (2001) J Catal 204: 378; Johánek V, Schauermann S, Laurin M, Gopinath CS, Libuda J, Freund H-J (2004) J Phys Chem B 108:14244
12. Somorjai GA, Yang M (2003) Top Catal 24(1–4):61 and references therein
13. Piccolo L, Becker C, Henry CR (2000) Appl Surf Sci 164:156; Piccolo L, Henry CR (2001) J Mol Catal A: Chemical 167:181; Judai K, Abbet S, Wrz AS, Heiz U, Henry CR (2004) J Am Chem Soc 126:2732
14. Henry CR (1998) Surf Sci Rep 31:23 and references therein
15. Wallace WT, Goodman DW (2006) In: Richards R (eds) Surface and nanomolecular catalysis, CRC Pr I Llc., p 337; and references therein
16. Choi Y-K , Zhu J, Grunes J, Bokor J, Somorjai GA (2003) J Phys Chem B 107:3340
17. Kónya Z, Puntes VF, Kiricsi I, Zhu J, Ager JW, Ko MK, Frei H, Alivisatos P, Somorjai GA (2003) Chem Mater 15:1242
18. Bowker M, Holroyd RP, Sharpe RG, Corneille JS, Francis SM, Goodman DW (1997) Surf Sci 370:113
19. Pradeep T, Hegde MS (1991) Proc Ind Acad Sci (Chem Sci.) 103:591
20. Zaera F (2002) Int Rev Phys Chem 21:433
21. Libuda J (2005) Chem Phys Chem 5:625; Libuda J, Freund H-J (2005) Surf Sci Rep 57:157

22. Kleyn AW (2003) Chem Soc Rev 32:87
23. Nakao K, Ito S, Tomishige K, Kunimori K (2005) J Phys Chem B 109:17553; *ibid*, J Phys Chem B 109:24002
24. Thirunavukkarasu K (2006) Molecular beam studies of nitric oxide reduction reactions on Pd(111) surfaces Ph.D. Thesis University of Pune
25. Taylor KC (1993) Catal Rev Sci Eng 3:457; Shelef M, Graham GW (1994) Catal Rev Sci Eng 36:433; Kreuzer T, Lox SE, Lindner D, Leyrer J (1996) Catal Today 29:1
26. Ramsier RD, Gao Q, Waltenburg NH, Lee K-W, Nooij OW, Leerts L, Yates Jr JT (1994) Surf Sci 320:209; Ramsier RD, Gao Q, Waltenburg NH, Yates Jr JT (1994) J Chem Phys 100:6837
27. Schauermann S, Johánek V, Laurin M, Libuda J, Freund H-J (2003) Phys Chem Chem Phys 5:5139
28. King DA, Wells MG (1972) Surf Sci 29:454
29. Clausing P (1932) J Vac Sci Tech 8(5):636
30. Pauly H (1988) In: Scoles G (ed) Atomic and molecular beam methods, vol 1. Oxford University Press, p 99
31. Scoles G (1988) In: Scoles G (ed) Atomic and molecular beam methods, vol 1. Oxford University Press, p 1
32. Thirunavukkarasu K, Thirumoorthy K, Libuda J, Gopinath CS (2005) J Phys Chem B 109:13272
33. Thirunavukkarasu K, Thirumoorthy K, Libuda J, Gopinath CS (2005) . J Phys Chem B 109:13283
34. Campbell CT, Valone SM (1985) J Vac Sci Technol A 3: 408
35. Guevremont JM, Sheldon S, Zaera F (2000) Rev Sci Instrum 71:3869
36. Fisher GL, Meserole CA (2005) J Vac Sci Technol A 23: 722
37. Liu J, Xu M, Nordmeyer T, Zaera F (1995) J Phys Chem 99: 6167
38. Conrad H, Ertl G, Koch J, Latta EE (1974) Surf Sci 43:462
39. Thirunavukkarasu K, Nagarajan PS, Gopinath CS, Prasad SD (In Preparation)
40. Burghaus U, Jones IZ, Bowker M (2000) Surf Sci 454–456:326
41. Sharpe RG, Bowker M (1996) Surf Sci 360:21
42. Bowker M, Bennett RA, Jones IZ (2004) Top Catal 28:25
43. Rainer DR, Vesecky SM, Koranne M, Oh WS, Goodman DW (1997) J Catal 167:234
44. Prevot G, Henry CR (2002) J Phys Chem B 106:12191
45. Prevot G, Meerson O, Piccolo L, Henry CR (2002) J Phys Cond Matt 14:4251
46. Gopinath CS, Zaera F (2000) J Phys Chem B 104:3194